CrossMark

ORIGINAL RESEARCH

Springback prediction and reduction in deep drawing under influence of unloading modulus degradation

Hamad ul Hassan[1] · Fawad Maqbool[2] · Alper Güner[1] · Alexander Hartmaier[3] ·
Nooman Ben Khalifa[1] · A. Erman Tekkaya[1]

Abstract Springback is considered as one of the major problems in deep drawing of high-strength steels (HSS) and advanced high-strength steels (AHSS) which occurs during the unloading of part from the tools. With an ever increasing demand on the automotive manufactures for the production of lightweight automobile structures and increased crash performance, the use of HSS and AHSS is becoming extensive. For the accurate prediction of springback, unloading behavior of dual phase steels DP600, DP1000 and cold rolled steel DC04 for the deep drawing process is investigated and a strategy for the reduction of springback based on variable blankholder force is also presented. Cyclic tension compression tests and LS-Opt software are used for the identification of material parameters for Yoshida-Uemori (YU) model. Degradation of the Young's modulus is found to be 28 and 26 and 14 % from the initial Young's modulus for DP600, DP1000 and for the DC04 respectively for the saturated value. A finite element model is generated in LS-DYNA based on the kinematic hardening material model, namely Yoshida-Uemori (YU) model. The validation of numerical simulations is also carried out by the real deep drawing experiments. The springback could be predicted with the maximum deviation of 1.1 mm for these materials. For DP1000, the maximum springback is reduced by 24.5 %, for DP600 33.3 and 48.7 % for DC04 by the application of monotonic blankholder force instead of a constant blankholder force of 80 kN. It is concluded that despite the reduction of Young's modulus, the springback can be reduced for these materials by increasing the blankholder force only in last 13 % of the punch travel.

Introduction

In the last decade in the automotive industry, the development of lightweight but crash-resistant cars has been a primary concern, the main reason being the environmental issues and the introduced safety regulations. The use of high-strength steel (HSS) and advanced high-strength steel (AHSS) has been considered as one of the possible solutions to this challenge. Such materials have the ability to make lighter cars while at the same time the crash resistance of the vehicles can be maintained. However a fatal problem in the application of HSS and AHSS is the springback which affects the dimensional accuracy of formed products directly.

Springback is mainly elastic deformation which occurs when the tool is removed. The crux of the earlier researches comes out to be the fact that the final shape of the part depends on the amount of elastic energy stored in the part during the process of sheet metal forming [1]. Classical theory of plasticity predicts linear-elastic unloading after the plastic deformation with stiffness being equal to that of the Young's modulus. In reality this unloading is non-linear and there is a considerable decrease in the elastic stiffness and with increasing plastic strain and this variation of Young's modulus can produce a significant difference in the springback prediction.

✉ Hamad ul Hassan
hamad.hassan@iul.tu-dortmund.de

[1] Institute of Forming Technology and Lightweight Construction, TU Dortmund, 44227 Dortmund, Germany

[2] Department of Design and Manufacturing, Brandenburg University of Technology, 03046 Cottbus, Germany

[3] Interdisciplinary Centre for Advanced Materials Simulation, Ruhr-University Bochum, 44801 Bochum, Germany

 Springer

Read [2] pointed out for the first time that the small reversible displacement of dislocations caused by an applied stress contributes to the non-elastic strain. Hence a decrease of the modulus is caused and this motion of dislocations results in dissipation of energy and increase of the internal friction. Both macroscopic and microscopic measures were adopted for the investigation of the influence of plastic deformation on elastic modulus [3]. It is concluded that main sources for the decrease of the elastic modulus are the movement of the mobile dislocations and dislocation pileup.

The change of elastic modulus with the increase of plastic strain was first investigated by Lems [4] and stated that the point defects and dislocations are the main cause of this change. It is explained that the saturation of the elastic modulus with two models based on the representation of the dislocation by an elastic string the other based on the kink movement. More recently Morestin et al. [5] used a uni-axial tensile test during the loading process for the investigation and stated work hardening as a possible cause of appreciable decrease in the Young's modulus and that this property diminishes with increase of plastic strain. It was observed that this diminution can reach more than 10 % of the initial value after only 5 % plastic strain.

Cleveland and Ghosh [6] explained that the springback strain is an elastic strain which develops during loading and unloading and hence leads to a hysteresis behavior (energy loss) in metals. The magnitude of springback is roughly proportional to the ratio between the magnitude of residual stress which occurs after forming and the elastic modulus of material. This phenomenon is particularly problematic in case of high strength steels because of the resulting high residual stresses. It is also found that the slope of the elastic modulus variation was different during loading and unloading due to the those micro-plastic strains, which fail to overcome the barriers set up due to the generation of new dislocation network during loading and unloading.

Eggertsen and Mattiason [7] presented that the predicted springback is greatly impacted by the degradation of elastic stiffness due to plastic straining. The pre-strain effect on springback of a dual phase steel is studied experimentally by Kim and Kimchi [8] for an S-rail stamping test. The magnitude of springback is found to be significantly influenced by the deformation histories of steel parts. Verma et al. [9] stated that for the cases when deformation of blank sheets increases, the dependency of elastic modulus on plastic strain could have a considerable effect on the springback of material. Therefore, in each forming step, the forming history is one of the key factors for the springback effect.

The dependency of the elastic modulus on plastic strain is also discussed by Fleischer et al. [10]. It is shown that the influence of elastic modulus on springback behavior becomes especially higher when large deformations occur in steel sheets during the forming process. Furthermore, HY [11]

noticed the non-linear behavior in the elastic part of a stress–strain curve obtained during unloading. Nevertheless, this non-linear behavior of unloading and reloading curves could be neglected. Chongthairungruang et al. [12] observed from the unloading–reloading curves that the total strain recovery during unloading stage decreases when plastic strain becomes higher and finally reaches a saturation value. It is however observed that there can be up to 22 % reduction in the initial Young's modulus with increasing plastic strains for HSS [6]. Zhu et al. [13] found that the change in the elastic modulus decreased from 6 to 12 % for mild steels and from 9 to 25 % for AHSS for the increase of strain from 0.01 to 0.05.

Further, for an accurate springback prediction in sheet metal forming it is very important to thoroughly understand the hardening models, which describe proper material behavior. Yoshida et al. [14] proposed a new material model which considers the decrease in elastic modulus, transient softening, kinematic hardening, and the Bauschinger effect based on the cyclic tension-compression test at large strains for AHSS. The model is based on the two surface modeling scheme i.e. a yield surface moves kinematically within a bounding surface. Kinematic hardening is assumed for the yield surface and mixed isotropic-kinematic hardening for the bounding surface. In this model, isotropic hardening for bounding surface represents the global work hardening therefore a non-isotropic hardening for bounding surface is used to represents the work hardening stagnation caused during the reverse flow due to dissolution of dislocation cell walls. Plastic region for work hardening stagnation increases with encompassed plastic strain. This is represented by expansion of non-isotropic hardening surface with plastic strains. Zang et al. [15] investigated these effects along with degradation of Young's modulus for their effect on springback and concluded that Young's modulus has the largest effect on springback prediction by finite element analysis (FEA) and the use of initial value of Young's modulus leads to the underestimation of the springback. The results for DP700 showed that the consideration of unloading modulus is more important than the Bauschinger effect and transient behavior, and permanent softening in springback prediction. Eggertsen and Mattiason [16] investigated springback in deep drawing for materials DP600, DX56 and 220IF with different hardening laws. It was concluded that the influence of this effect was even bigger than that of the choice of hardening law. Simulated springback was smaller than the corresponding experimental ones for the case when the effect of elastic stiffness degradation due to plastic loading was not included in the predictions. Kim and Kimchi [8] found that simulations using variable elastic modulus provide more precise springback prediction than the ones using constant elastic modulus. However, there are presently insufficient data available concerning the springback prediction of dual phase steels under consideration of elastic modulus change relating to the pre-strain effect.

However, since the amount of stored elastic energy depends on a number of parameters, prediction of springback proves to be a complicated task. Also the sensitivity of springback prediction to the numerical parameters of finite element (FE) simulation adds further challenge to this complexity [17]. Springback is also affected by a number of geometrical parameters and material parameters, however once the design is finalized with reference to a certain material, only the different combinations of the process parameters could be used to cope with the problem of springback. Different time varying process parameters like blankholder force (BHF), friction and drawing velocity also show a profound effect on the springback. Because of the sensitivity of springback prediction to the numerical parameters of finite element (FE) simulation, the complexity is further increased. Along with the other numerical parameters which influence springback, the type, order and integration scheme of finite elements as well as the shape and size of the finite element mesh, play a vital role for the accurate prediction of springback [18].

Samuel [19] brought to light the dependency of springback effect on friction and side wall curl on blank holder force. It is found that the higher value of friction coefficient decreases springback and side wall curl by increasing tension in strip wall based on the blankholder force. The increase in the level of blankholder force causes the restraining forces to increase, which in turn cause the reduction of stress inhomogeneities along the sheet thickness, hence leading to decrease in elastic springback. By increasing the restraining force the above mentioned targets could be achieved. Papeleux and Ponthot [20], Ledoux et al. [21], De Souza et. al [22], D'Acquisto and Fratini [23] studied the influence of several physical and numerical parameters on springback including the BHF. Improvements in a bad shape can be made by applying the variable blank holder force (VBHF) that will change the wall tension in the process of bending [24]. Cao et al. [25] also proposed a stepped binder force trajectory algorithm by neural network controller, where the stepped variable blank holder force (VBHF) trajectory was determined using the neural network controller. Schmoeckel and Beth [26] have shown that a blankholder pressure control dependent on drawing depth is quite beneficial for the reduction in springback. They observed that a sudden increase in blankholder pressure at the end of the forming process proved to be particularly beneficial for the springback reduction. Liu et al. [27, 28] developed the simple closed-loop type algorithm for VBHF trajectory. In their method, the forming limit diagram (FLD) was employed to avoid tearing through the forming process. The major problem in these cases is the exact determination of the values of blankholder forces and the moments of variation during the process. In the previous work of authors [29], an extended FE model has been presented which is capable to accommodate the functional input for blankholder force and friction coefficient. The effect of these process parameters over the punch

travel has been analysed. It is found that a higher value of these parameters for the last 13 % of the punch travel has a significant effect on the reduction of springback in final part.

With ever continuing advancements in the material technology and developments of new materials, the need of accurate springback prediction also becomes more profound. It can be concluded that a suitable material model which encompasses all the relevant states of forming and the degradation of Young's modulus should be used for the better prediction of springback especially for AHSS. This work covers the investigation of springback prediction for the deep drawing for the materials DC04, DP600 and DP1000. It is observed that all these materials exhibit a significant amount of reduction in the elastic modulus before reaching a saturation value and that should be taken into account for the accurate prediction of springback in deep drawing. The incremental analysis of the effect of variation of blankholder force on the springback reduction is also presented. Since the blankholder force causes stretching in the sheet and is directly related to the material flow in the die, to obtain the desired forming result, this time varying process parameters should be controlled in an optimum manner. This proper variation of blankholder force during process will counter the effect of this degradation and will lead to a reduction in springback.

Cyclic tension-compression tests

Cyclic tension-compression tests are carried out to determine the stress-strain response of the three different steels DP1000, DP600 and DC04 with thickness of 1 mm and with 3 repetitions for all the specimens. Specimen is clamped between two mechanically operated arms as shown in Fig. 1.

A strain rate of 0.01/s is used. A displacement control program is applied to control the movement of the arms and apply the displacement. The standard uniaxial tensile test is one of the most commonly used testing methods to characterize the hardening behavior of a material. The current tests are a modified form of a standard uni-axial tensile test. The standard test is not used because of its buckling tendency. In these tests, gauge length is kept small in order to overcome the buckling. The advantage is the ease in calculation of material behavior by analytical equations due to the uniaxial stress state. The specimen is shown in the Fig. 2. The specimen has an active gauge length of 2 mm, width of 2 mm and thickness of 1 mm.

Due to the small gauge-length application of an extensometer is not possible and the strains are measured by the optical measurement instrument. The system records the deformation of the specimen from the start till end of the experiment based on the deformation of the sprayed stochastic pattern. The strain measuring accuracy (in %) of the system is up to 0.005. Two different loading schemes are used. A tension-unloading scheme without going into the compression phase
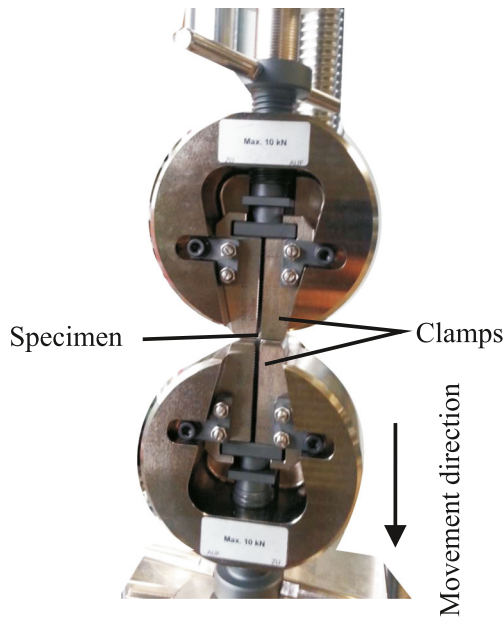
Fig. 1 Tool setup for tension-compression test

for the quantification of Young's modulus and the tension-unloading-compression scheme for the generation of cyclic stress-strain curves used for finding the parameters of Yoshida-Uemori model. A monotonic uni-axial tensile loading for the mixed isotropic-kinematic hardening of bounding surface [14] yields

$$\sigma_{bound} = B + (R_{SAT} + b)(1-e^{-m\epsilon_p}) \tag{1}$$

Where B represents the initial size of the bounding surface, R_{SAT} and b gives the saturation size of the bounding surface with b being the kinematic hardening part and R_{SAT} being representing the isotropic hardening part and m is the isotropic
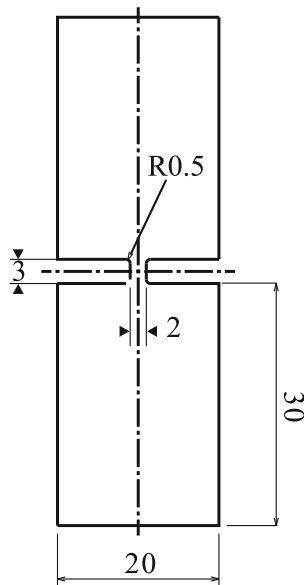

Fig. 2 Specimen geometry for tension-compression testing (dimensions in mm)

hardening component similar to Voce. The other material parameters of Yoshida-Uemori model are C and h where C describes the transition behavior between elastic and plastic deformation and h is used to fit the hardening stagnation with experimental results describes the hardening stagnation.

For this case two cycles of tension, unloading and compression are undergone due to the reason that during deep drawing some region of the part undergoes such cyclic loading of tension compression and again followed by tension. In order to do a more realistic simulation and the generation of more accurate material parameters, this curve is used as a target curve for the identification of material materials. True stress-strain curves obtained as a result of the above mentioned loading scheme are presented in the Fig. 3. In Fig. 3, results (a), (c) and (e) are utilized for the quantification of the degradation of the Young's modulus for three materials. Results (b), (d) and (e) represent the cyclic behavior of the DC04, DP600 and DP1000 respectively.
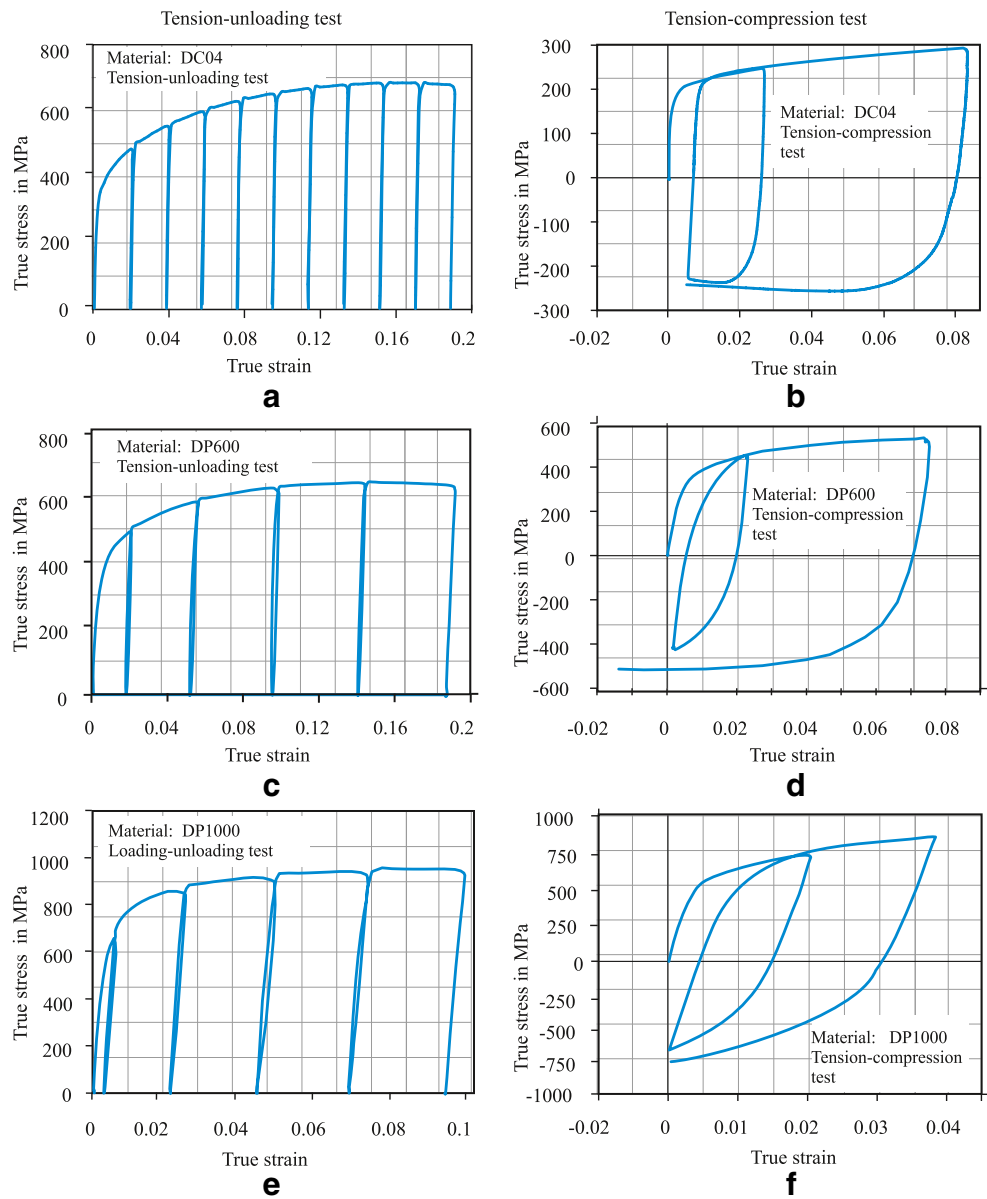
An alternation of the loading is not carried out for the calculation of unloading modulus, due to the problem of buckling in the compression regime for these tests. In Fig. 3 (a), (c) and (e) only the unloading is carried out and the compression regime is not followed. The reason for that is the fact that the unloading modulus with the increase in plastic strain is needed to be characterized which can be done even without going into compression. However, in order to characterize the kinematic hardening behavior of the sheet as shown in the Fig. 3 (b), (d), (f) the load reversal is carried out to capture the Bauschinger effect, work hardening stagnation for the case of DP600 and even permanent softening for DC04. The transition region for DP1000 is also captured successively. Since only two cycles are carried out, the compression region is also followed.

These curves are used as target experimental curves for material parameter identification scheme for the Yoshida-Uemori model. For all the materials, the Bauschinger effect can be seen. This effect is more dominant for DP1000 and DP600 as compared to DC04 which is due to their differences in the flow stress. In the tension compression tests, DP600 shows the work hardening stagnation at the end of unloading while DP600 shows workhardening stagnation. DP1000 shows a strong Bauschinger effect and the transition region is also large. For the cyclic tests, DP1000 is strained to 0.04 only because of very strong tendency to buckling.

Since the springback takes places during the unloading of part, therefore unloading-modulus is important for springback simulations. Loading modulus and unloading modulus are different from each other because the elastic loading and unloading curves from stress-strain diagrams show a hysteresis behavior as seen in Fig. 3. Measurement of the degraded value of Young's modulus is actually the measurement of the slope of the unloading curve from the stress-strain diagram.

Unloading modulus in this work is calculated by joining the point of maximum stress σ_1 with the point of minimum

Fig. 3 True stress-strain curves for DC04, DP600 and DP1000

a Material: DC04 Tension-unloading test

b Material: DC04 Tension-compression test

c Material: DP600 Tension-unloading test

d Material: DP600 Tension-compression test

e Material: DP1000 Loading-unloading test

f Material: DP1000 Tension-compression test

stress σ_0 with a straight line for three materials DP600, DC04 and DP1000 (Fig. 4). The slope of this line is the apparent Young's modulus or unloading modulus.

The implementation of this "unloading modulus" in FE simulations requires a mathematical model. This mathematical variation in the Young's modulus was proposed by Yoshida et al. (2002) and is given by the following equation

$$E = E_0 - (E_0 - E_a)[1 - exp(-\zeta p)] \qquad (2)$$

Where E_0 is the initial Young's modulus and E_a is the value of Young's modulus at infinitely large plastic strains. E_a is called the saturated modulus i.e. no further decrease in the value of Young's modulus takes place. ζ is a material parameter controlling the rate of the decrease of the Young's modulus. This mathematical model will be defining the degradation

of the Young's modulus for FE simulations and these three parameters are the necessary input for the FE simulations.

The experimentally measured data i.e. degradation of Young's modulus is used to obtain the degradation rate for
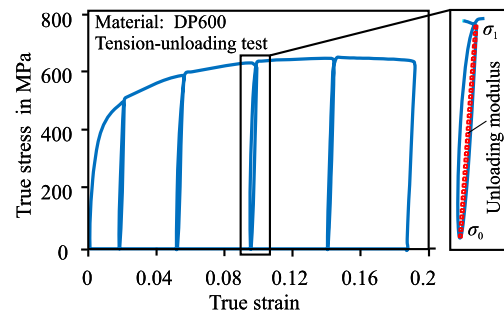

Material: DP600 Tension-unloading test

Fig. 4 Measurement of the unloading modulus

the materials and curve fitting is used to show the tendency of saturation for these materials. This is represented in the Fig. 5(a), (b) and (c) for DC04, DP600 and DP1000 respectively. From the figure it can be seen that the degradation in the apparent Young's modulus for DC04 is 15 % from the initial state to pre-strain of 0.12. Straining the specimen further did not resulted in a decrease of the Young's modulus and the saturated value of the Young's modulus is 186 GPa. However, degradation in the apparent Young's modulus for DP600 is 28 % from the initial state to pre-strain of 0.12. Straining the specimen further did not produce a further decrease of the Young's modulus and the saturated value of the Young's modulus is 147.6 GPa. DP1000 is pre-strained only to 0.1 and the higher pre-strain is not achieved due to the strong tendency of

buckling of the specimen. For DP1000, the degradation in the apparent Young's modulus for DP1000 is 26 % from the initial state to pre-strain of 0.09 with the saturated value of the Young's modulus being 156 GPa. The degradation in the apparent Young's modulus for DP600 and DP1000 is comparable but that of DC04 is quite less which is due to the difference in the strength of the materials. Due to the number of cycles for tension and unloading, the buckling effect arises. It is due to this buckling effect at the higher strain that a little drop in stress could be seen for DC04 and DP600. It is also due to this reason that the alternation of loading in not performed for the measurement of degradation of Young's modulus. It can be further observed that the saturation of Young's modulus degradation already reaches its saturation value at the pre-strain of 0.12 for DC04 and DP600.

In the next step the experimental tension-compression curves are used to find the parameters for Yoshida-Uemori (YU) model. All the three materials DC04, DP600 and DP1000 are used for the analysis. The simulation curves are generated by the application of same loading schemes to a 1-element based FE-model and the curve mapping is carried out for the determination of material parameters.

An initial tensile loading up to the strain of 0.02 is applied for all the 3 materials and then the unloading in carried out followed by the compression. A subsequent reloading is done till strain of 0.08 for DC04, 0.07 for DP600 and 0.04 for DP1000. The curve mapping of experimental curves with the simulation curves of cyclic loading is carried out using the LS-OPT optimization tool.

In the process of curve mapping, the experimental curve is set as a target curve and the same loading conditions are applied to the 1-element model for the determination of material parameters. The parameters are optimized for a minimum deviation between the simulation based and experimental curve. A polynomial based metamodel of linear order along with the D-optimal point selection is used for space sampling and number of simulation points is set to 16. Domain reduction (SRSM) based metamodel is selected for optimization. Deviation of both curves is given as objective function and the minimization of this objective function is used for optimization. Figure 6 shows the comparison of the experimental and numerical curves.

The selected parameters and their selected ranges are C between 250 and 1000, B (MPa) between 250 and 1000, R_{sat}(MPa) between 200 and 900, m between 20 and 100, h between 0 and 1 and b (MPa) between 200 and 900. Uniform set of parameters and the ranges are selected for all materials. The parameter Y representing the flow stress is taken directly from the results of uniaxial tensile test.

Material parameters of Yoshida-Uemori hardening model obtained by this curve matching for DC04, DP600 and DP1000 are listed in Table 1.
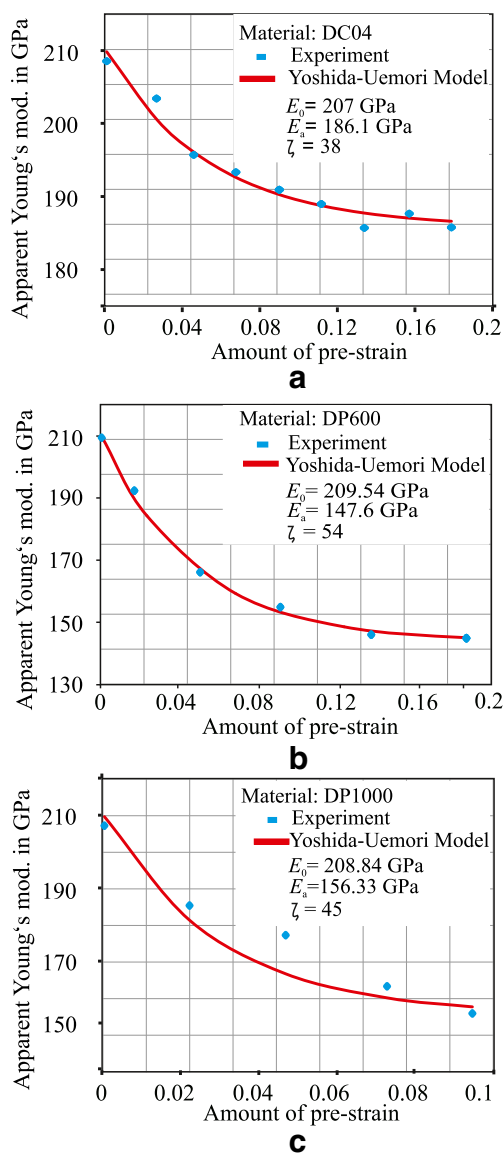

Fig. 5 Apparent Young's modulus degradation with pre-strain for **a)** DC04, **b)** DP600 and **c)** DP1000
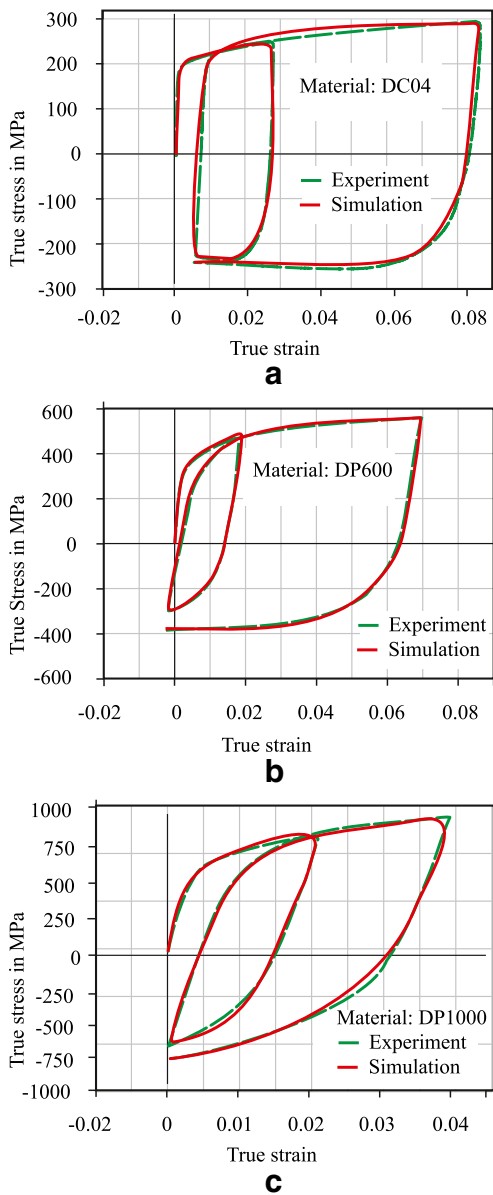
Fig. 6 Comparison of experimental and simulated true stress vs. true strain curves a) DC04, b) DP600 and c) DP1000

Numerical model for Deep drawing

Figure 7a shows a sketch for deep drawing of hat geometry. The important dimensions are shown in Fig. 7b for the die, punch, and blank holder. Due to the symmetry, the numerical analysis of the deep drawing process is performed by using only half of 3D numerical model to reduce the computational time. The size of blank is given by 50 mm*160 mm and the thickness is kept to be 1 mm. The clearance between punch and die is 1.18 mm with 0.18 mm used as drawing clearance.

For the analysis of deep drawing and springback, the FEM model using LS-DYNA is generated to investigate the effect of reduction of elastic modulus on the springback and its reduction by controlled material flow. The material is modeled

Table 1 Identified material parameters of Yoshida-Uemori hardening model

Parameter	DC04	DP600	DP1000
Y in MPa	180	310	645
C	425	475	887
B in MPa	700	510	695
R_{sat} in MPa	700	610	699
m	56	65	69
h	0.69	0.75	0.889
b in MPa	300	390	780

using the built-in material model from the LS-DYNA material library i.e. Yoshida-Uemori (YU) model. In this simulation model the die, punch and blankholder are modeled as rigid bodies. The sheet is modelled after a mesh convergence analysis with a total of 8000 elements and 1 mm of element size. Fully integrated shell elements (type 16) are used for the simulation of deep drawing and springback with 7 integration points over the thickness.

The deep drawing process is simulated with explicit time integration scheme while springback is simulated with implicit time integration scheme for the purpose of convergence. The maximum deviation in mm in each case is taken as the springback in the simulations.

This FE model is extended to accommodate the possibility of functional inputs, that is, the blank-holder force and the friction coefficient can be modeled as functions of time which in turn means the function of punch displacement.

To achieve such functionality, a Linux shell script has been developed which can be seen in Fig. 8. In conventional simulations, the blankholder force is kept constant. In the currently used model however, the blankholder force would be defined as a time varying parameter. This approach can also be used to change the values of other parameters in any specific
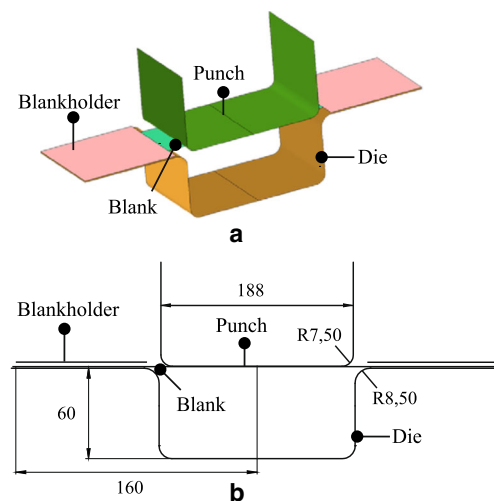

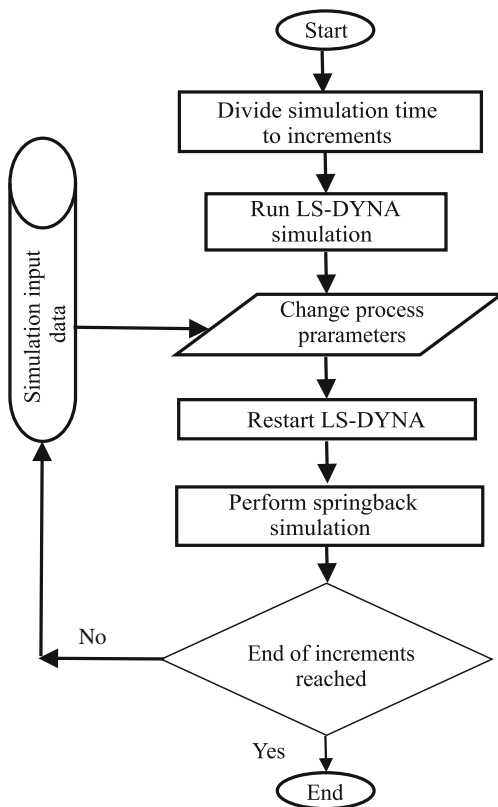**Fig. 7** Schematic diagram of the tool setup (dimensions are in mm)

Fig. 8 Shell script flowchart for the incremental calculation of springback

area of the same model for the generation of tailored properties over the surface of part. It starts and stops the simulation in a predefined manner and then changes the value of the blankholder force according to the statistical experimental designs. The entire drawing process is divided into a predefined number of increments and it is possible to change the value of the process parameters in any increment.

This also gives the possibility of implementation of different functions. After the stamping simulation, implicit simulation is carried out for the springback. Then the meshed geometries in the loaded state (before the springback) and unloaded state (after the springback) are exported for comparison with the experimental results. The average springback is calculated as the average deviation of all the nodes in the loaded and unloaded configuration. At the end of the punch travel the surface comparison is also done for the measurement of geometrical deviations and imperfections. Such an analysis also makes it possible to investigate evolution of other sheet metal failures over the punch travel and just not analyzing them at the end of the process.

Results and discussion

As mentioned in the earlier section, the material of sheet is modeled using the built-in material model from the LS-

DYNA material library i.e. Yoshida-Uemori (YU) model. For preliminary analysis, different FE simulations are run with constant blankholder force of 40 kN with the material DP600 by keeping the initial Young's modulus E_0 constant at 210 GPa and changing the respective degraded Young's modulus value in terms of percentage of initial Young's modulus i.e. 100 % meaning no degradation, 90, 70 and 50 % degradation in the value of initial Young's modulus. For the kinematic hardening, the material parameters found through the characterization for the Yoshida-Uemori hardening model for DP600 are used in these simulations. A curve fit is done for each case to determine the rate of decrease of the Young's modulus ζ. All other numerical and geometrical parameters are kept constant for these FE simulations (Table 2).

Four different FE simulations are run with varying intensity of Young's modulus degradation. Resulting deformed geometries after the springback simulations for these different cases are plotted in the Fig. 9. Experiment under the same condition as that of these simulations are performed. Experimental result of DP600 performed under the same conditions i.e. same blank holder force and coefficient of friction is plotted along with the FE deformed geometries in the Fig. 9. All numerical parameters and geometrical parameters are kept constant. The scatter of the deformed geometries is obtained by only changing degraded Young's modulus. It shows importance of using correct degraded Young's modulus in FE simulations. Springback increases with an increase in the degradation of the Young's modulus as can be seen in the Fig. 9. There is a large deviation in the values of springback, especially the side wall curl is much more pronounced for simulations with large degradation in Young's modulus. It can be seen that the experimental geometry lies very near to the simulation with 30 % reduction of the Young's modulus. From material characterization, degradation in the Young's modulus value for DP600 is found out to be 28 % which confirms the results. The simulation with constant Young's modulus underestimates the springback and for accurate prediction of springback this effect should be included in the simulation. It is shown from the FE simulations that not only it is very important to implement the degradation of the Young's modulus for FE simulations for accurate springback prediction but also the exact percentage of the degradation of the Young's modulus is very important.

Table 2 Springback for different degraded moduli keeping the initial Young's modulus constant

Case	E_o(GPa)	E_a(GPa)	ζ	Springback in mm
Case 1	210	210	0	12
Case 2	210	189	38	13.5
Case 3	210	147	54	17.2
Case 4	210	105	43	24

Fig. 9 Effect of intensity of Young's modulus degradation on springback
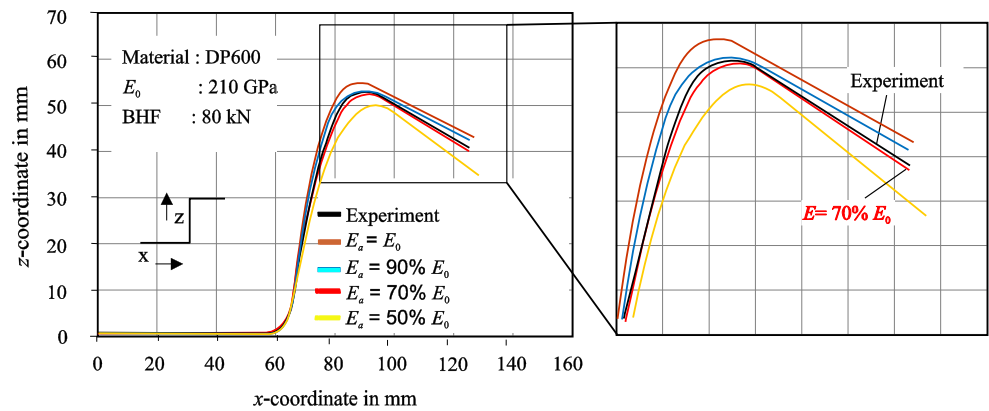
In order to investigate the accuracy of springback prediction for three different materials, blankholder forces of 40 kN and 80 kN are used for the deep drawing. There is no direct method for the measurement of coefficient of friction during the experiments; however the values used in simulations are based on the strip tensile tests. The deformed geometries from the deep drawing experiments are measured with the help of optical measurement system which creates a triangular mesh of the part. The geometries are sprayed in white and the images are captured at different angles from the camera which generates the mesh based on the captured images. The mesh from the simulation is compared with the mesh from experiment and geometric deviation between the two meshes can be seen in the form of a deviation fringe. Since in FE simulation a symmetry plane is used and only half geometry is modeled, therefore half geometry is used for the comparison so the deviation fringes can only be seen on the half portion in figures. Deviations are plotted in the form of a fringe in the units of mm.

All the FE springback simulations are carried out using the Yoshida-Uemori hardening model with the calculated material parameters and taking degradation of Young's modulus into account. A sectional plot of the deformed geometries under 40 kN of constant blankholder force after the springback simulations are presented in the Fig. 10.
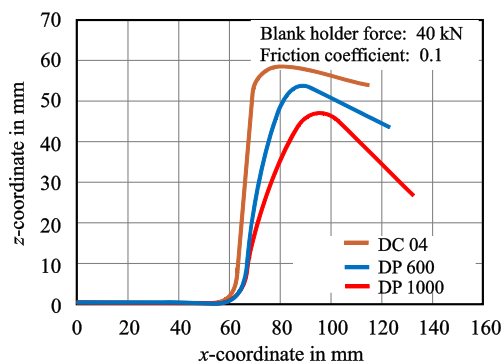
Figure 10 shows that the higher the strength, the more pronounced is the springback. Springback levels are highest for the DP1000 followed by DP600 and then DC04. This is because of the fact DP1000 has the highest elastic strains to be recovered after unloading, followed by DP600 and DC04. Figure 11 shows the image of the parts stacked together to show the springback for each material.

The finite element simulations are validated experimentally for these materials under the same operating conditions. The results of the comparison of deformed geometries under a blankholder force of 40 kN are presented in Fig. 12. To further supplement these results, FE and experimental geometries drawn under a blank holder force of 80 kN are also compared and their results are shown in Fig. 13. Results are presented in the form of positive and negative deviations of FE mesh from experimental mesh in mm. A zero value of deviation means that the two meshes are perfectly aligned to each other. A positive deviation at a point means the springback values by FE analysis at that point is being under estimated and both geometries do not intersect. On the contrary, a negative deviation at a point means the springback value from FE simulation at that location is overestimated and both geometries intersect each other and FE geometry exceeds the experimental geometry by the amount of negative deviation in mm. In the simulation for blankholder forces of 40 kN and 80 kN for all the materials it is observed that the springback is under-predicted by the simulation with constant Young's modulus as compared to the one with the degraded Young's modulus. This is clearly understood by the fact that with the increasing plastic strain during the process, if the Young's modulus remains constant then at the end of the simulation the springback would be calculated based on this Young's
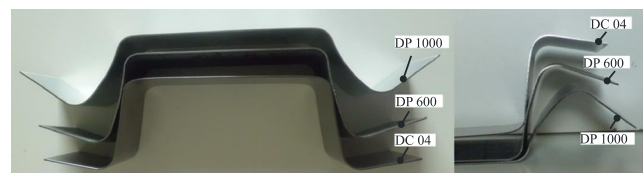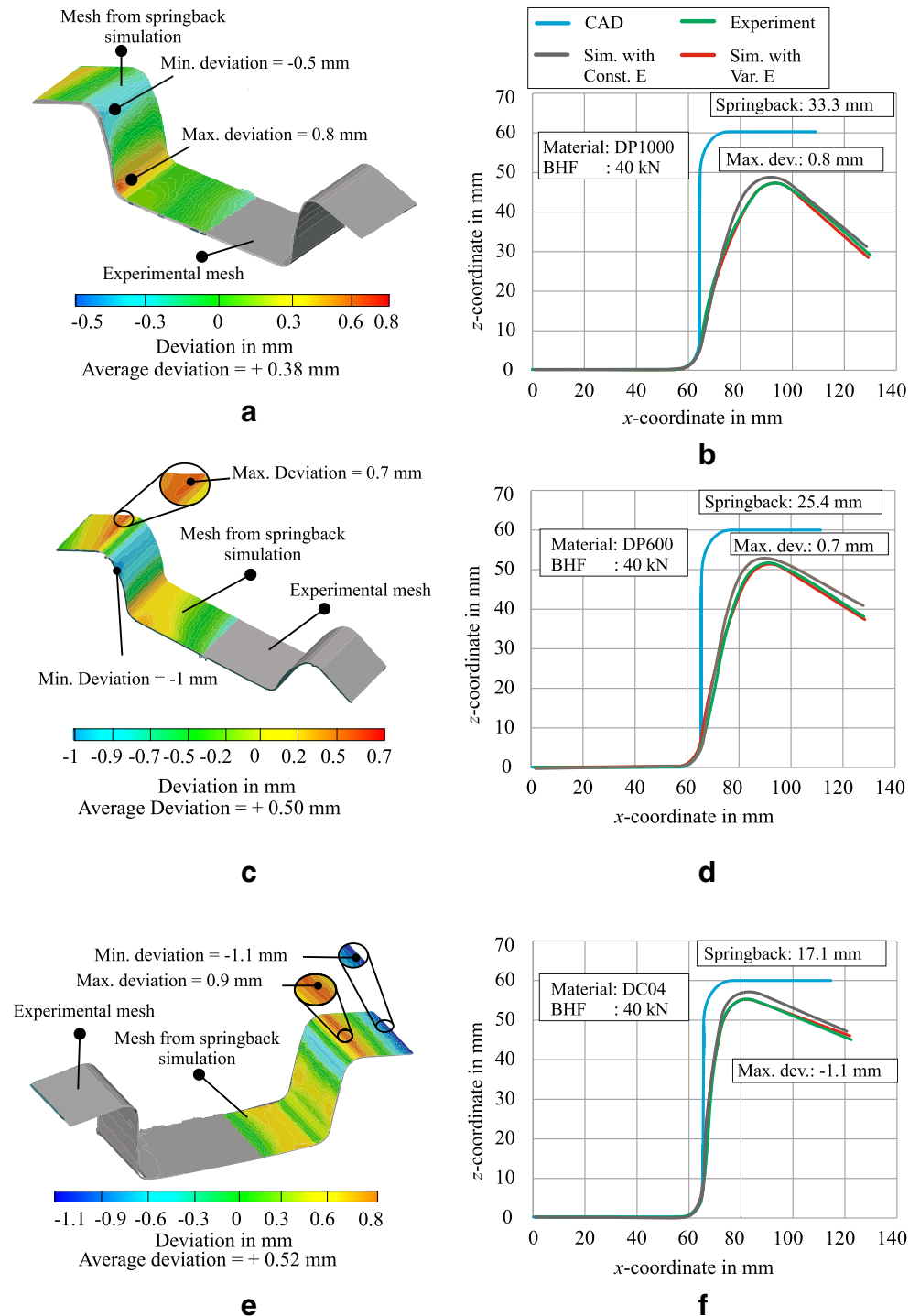

Fig. 10 Deformed geometries after springback for three different materials from FE simulations

Fig. 11 Deformed geometries after springback from experiments

Fig. 12 Geometrical comparison results for DP1000, DP600 and DC04 steels drawn under a blank holder force of 40 kN


a

b

c

d

e

f

modulus which would be smaller than the simulation with the springback which is degraded with the increasing plastic strain. This underestimation of springback for DC04 is 3.3 and 0.8 mm, for DP600 approximately 3 and 3.3 mm and for DP1000 it is approximately 1.4 and 3.06 mm for blankholder forces of 40 kN and 80 kN respectively.

Figure 12 represents the geometry comparison results for DP1000, DP600 and DC04 steels drawn under a blank holder force of 40 kN. For DP1000 the maximum and minimum deviation is +0.7 and -0.5 mm respectively. The average deviation between the experimental and simulation results is + 0.38 mm. For the case of DP600 the maximum and minimum deviation are +0.7 and -1 mm respectively. The average deviation between the experimental and simulation results is + 0.50 mm. For the case of DC04 under the same process conditions, the maximum and minimum deviation is +0.9 and -

Fig. 13 Geometrical comparison results for DP1000, DP600 and DC04 steels drawn under a blank holder force of 80 kN
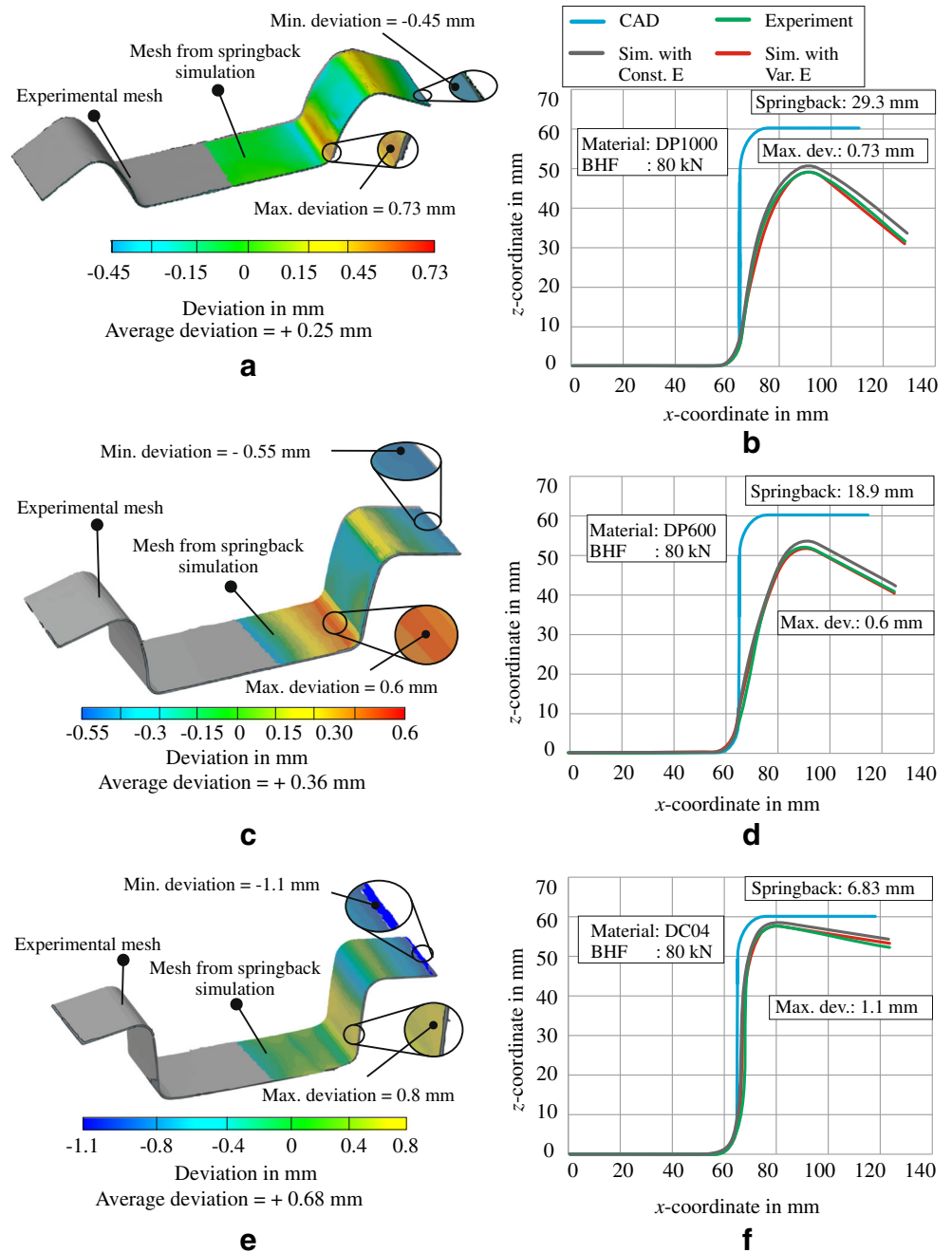
1.1 mm. The average deviation between the experimental and simulation results is +0.52 mm.

The geometry comparison is also carried out for a higher level of force of 80 kN for all the 3 materials and the results can be seen in Fig. 13.

In this case for the DP1000, the maximum and minimum deviations are +0.73 and -0.45 mm. The average deviation between the experimental and simulation results is +0.25 mm. For DP600, the maximum and minimum deviations are +0.6 and -0.55 mm. The average deviation between the experimental and simulation results is +0.36 mm. Similarly for DC04, the maximum and minimum deviation is +0.8 and -

1.1 mm. The average deviation between the experimental and simulation results is +0.6746 mm.

DP1000 has the highest amount of the springback for the three materials being investigated. The amount of experimental or actual springback is 33.3 and 29.3 mm for blank holder force of 40 kN and 80 kN respectively. DP1000 is AHSS and has the highest strength of all the materials being investigated. Young's modulus degradation is almost same as that of DP600 i.e. 26 % but the springback is more as compared to DP600. This is due to the strength of the material. DP600 also belongs to the family of AHSS. The springback is expected to be high. The amount of experimental or actual springback is 25.4 and

15.6 mm for blank holder force of 40 and 80 kN respectively. Young's modulus degradation is almost same as that of DP1000 i.e. 28 % but the springback is less as compared to DP1000. This fact confirms that with equal degradation of Young's modulus for two materials, the stronger material will have the higher springback. DC04 has the least amount of the springback from the three materials being investigated. The amount of experimental or actual springback is 17.1 and 6.83 mm for blank holder force of 40 kN and 80 kN respectively. DC04 is cold rolled steel and has the least strength of all the materials being investigated. Young's modulus degradation is less as compared to DP600 and DP1000 i.e. 14 %. Springback is expected to be less as compared to other two materials and this is confirmed by simulations as well as experiments. Springback reduces from 33.3 to 29.3 mm for DP1000, from 25.4 to 15.6 mm for DP600 and from 17.1 to 6.83 mm for DC04 for a similar increase of the blankholder force from 40 to 80 kN. A very small decrease in the springback for DP1000 is due to the fact that the stresses produced by 80 kN are also not high enough to generate the higher tension which can suppress the hardening of material at the later stage.

The geometry comparison results show a good match between numerical and experimental results and show a very small level of deviations for both cases of different blank holder force and despite such large springback the maximum deviation is not more than 1.1 mm. The springback is underestimated in the simulation for the cases when the degradation of Young's modulus is not included for all the materials and hence for the accurate prediction of springback it is necessary to include this effect. In order to counter this effect of degradation of Young's modulus a strategy for the reduction of springback is presented in the next section.

Strategy for springback reduction

Primarily the stretching in the sheet is caused by the blankholder force which directly influences the flow of material into die. This time varying process parameters should be controlled in an optimum manner for obtaining the desired forming result. Since the plastic strains increase with the process time which reduces the apparent Young's modulus and in turn increases springback, the proper variation of blankholder force during process will counters the effect of this degradation and will lead to a reduction in springback.

For the minimization of springback the strategy of variation of blankholder is adapted. Based on the literature survey it could be seen that the variation of blankholder force has a profound effect on the springback reduction. The profiles of the variable blankholder force used in the present work are shown in Fig. 14.
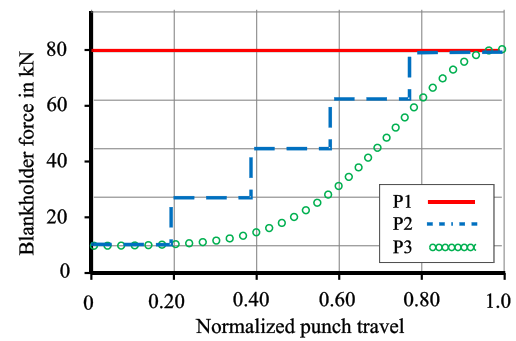

Fig. 14 Blankholder force profiles used in analysis for springback reduction

Profile 1 is the traditional constant blankholder force that is used in the industry and shows the maximum force that is used in the analysis. Profile 2 shows the monotonic stepwise variation of blankholder force which can be realized in the experiments. Profile 3 is the optimized blankholder force for the deep drawing based on the previous work of authors which however needs the servopress and cannot be realized experimentally in the available machine. In order to realize the experiments the profile 2 is used to generate the profile similar to the optimized one with stepwise increase in force. 5 steps of monotonic increase in the force are used to reach from the minimum to the maximum level. Another significance of the usage of 5 steps resides in the assumption that each step is responsible for the formation of certain area in the part.

Kitayama et al. [30] divided the complete punch travel in 6 parts and used an assumption that the first two parts are responsible for the forming of base, the next 2 parts responsible for the forming of wall and the last two parts are responsible for the formation of flange. It is a very good assumption however this doesn't account for the formation for top and bottom die radius which are very much important with reference to the investigation for springback reduction. In this work too each step in the stepwise increasing blankholder force profile is assumed to be responsible for a certain area. The first step is responsible for the forming of base, second step for bottom die radius, third for wall, fourth step for top die radius and fifth
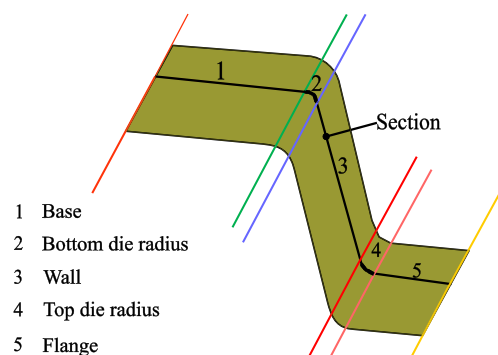

1 Base
2 Bottom die radius
3 Wall
4 Top die radius
5 Flange

Fig. 15 Different regions for forming of a U-geometry

step for forming of flange. This can be seen schematically in the Fig. 15.

In Fig. 16 the results of geometric deviation on a section are shown for different materials. It can be seen for all the cases irrespective of the material that the profile 3 gives the smallest springback. The springback in case of profile 2 is higher than profile 3 however for the experimental validation this profile is selected because of its ease in realization on the hydraulic press.

In Fig. 16(a), (b) and (c) the results of simulation for springback development over punch travel for the 3 different blankholder force profiles can be seen for DP1000, DP600 and DC04 respectively. It can be observed that the springback for profile 2 is smaller than that of the profile 1 for each

material, although the maximum force remains the same and the profile 2 uses the maximum blankholder force in only last 20 % of the punch travel. It can be seen that for all the 3 different materials the springback for profile 1 stays smaller in the beginning due to higher tension, however with the process time the hardening of the material tends to increase which leads to an increase in the springback at the later stage. For the profiles 2 and 3 we observe the opposite that the springback is higher in the beginning and the after 40 % of the punch travel it becomes smaller than P1 and stays smaller for the rest of the process.

For DP1000, the maximum springback is reduced from 29.3 to 22.1 mm, for DP600 from 18.9 to 12.6 mm and for

Fig. 16 Incremental springback development and section comparison for end springback
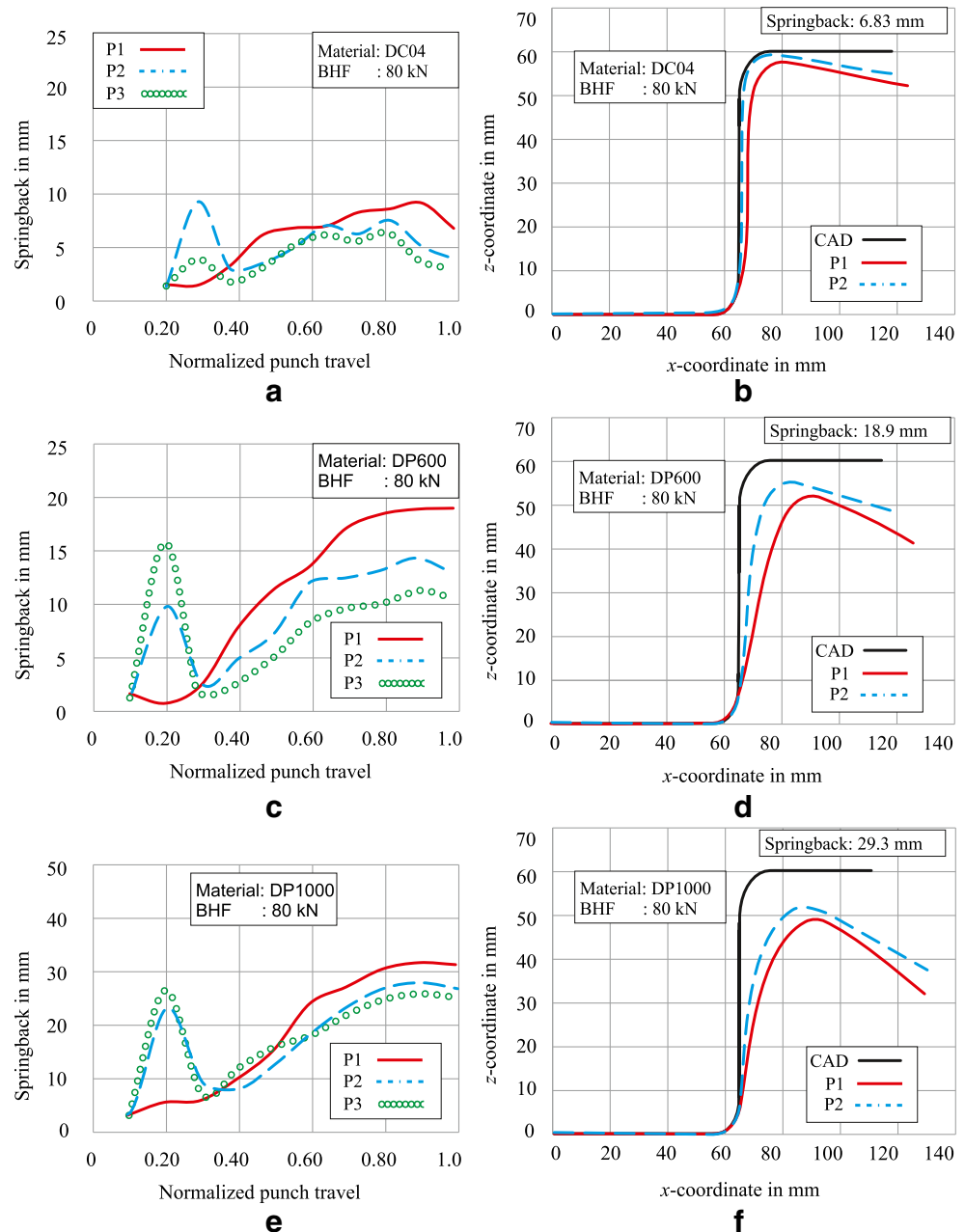
DC04 from 6.83 to 3.5 mm for the case of profile 3. In the Fig. 16(d), (e) and (f) comparison of the geometries on a section is carried out for the experiments using the profiles 1 and 2. Due to the experimental limitations the experiments for profile are not performed which requires a programmable servopress. The springback for profile 2 is a little higher than that of profile 3 because of earlier increase in the force due to monotonic profile. This springback can be further reduced if the maximum force is used in only last 13 % of the punch travel. This effect can be explained by the fact that the higher plastic strain leads to a higher reduction in the elastic modulus and thus resulting in a higher springback. Moreover the higher stretching forces in the beginning of the process leads to the hardening of the material which makes it difficult for the constant blankholder force to produce enough tension at the later stage. The springback in more pronounced in the flange region and the region of blankholder force responsible for bringing in the tension in this region is the last part. This describes the fact that the higher tension at in the last part of the drawing process reduces the springback quite dominantly.

Conclusions

This work focuses on the consideration of the degradation of Young's modulus in deep drawing and springback simulations and the variation of blankholder force during deep drawing for the reduction of springback for steels DC04, DP600 and DP1000. The validation of result is also done with the deep drawing experiments. Yoshida-Uemori hardening model is used for the FE simulations. Important conclusions are

- Degradation of Young's modulus is more pronounced for high strength steels DP600 and DP1000 as compared to the DC04. This degradation is 28 and 26 % for DP600 and DP1000 and 14 % for the DC04.
- With the increase of plastic strains to around 0.05, the degradation of Young's modulus is almost linear followed by a steady degradation with increasing the plastic strain until the saturation value is achieved. After that Young's modulus does not decrease further even by increasing plastic strain. A plastic strain range of 0.12 to 0.16 is enough for the quantification of the degradation of Young's modulus for these classes of material.
- FE simulations of U-geometry of three different materials i.e. DP1000, DP600 and DC04 having three entirely different magnitudes of springback are simulated using Yoshida-Uemori hardening model and taking degradation of Young's modulus into account. It is shown that the consideration of Young's modulus degradation is crucial for the accurate prediction of springback in deep drawing, especially for AHSS which show the reduction of around 28 % from the original Young's modulus.

- It is observed that the springback can be reduced if the maximum force is used only during last 13 % of the punch travel. Higher tension at the end of deep drawing leads to the same residual stresses however the reduction in Young's modulus is smaller which leads to smaller springback.

References

1. Narasimhan N, Lovell M (1999) Predicting springback in sheet metal forming: an explicit to implicit sequential solution procedure. Finite Elem Anal Des 33:29–42
2. Read TA (1941) Internal Friction of Single Crystals of Copper and Zinc. Transactions of the Americans institute of mining and metallurgical engineers. 143, Institute of metals division
3. Yang M, Akiyama Y, Sasaki T (2004) Microscopic evaluation of change in springback characteristics due to plastic deformation. International Conference on Numerical Methods in Industrial Forming Processes NUMIFORM, p 881
4. Lems W (1963) The change of Young's modulus after deformational low temperature and its recovery, Ph.D. Dissertation, Delft
5. Morestin F, Boivin M, Silva C (1996) Elasto plastic formulation using a kinematic hardening model for springback analysis in sheet metal forming. J Mater Proc Tech 56:619–630
6. Cleveland R, Ghosh A (2002) Inelastic effects on springback in metals. Int J Plast 18:769–785
7. Eggertsen PA, Mattiasson K (2009) On constitutive modeling of the bending-unbending behaviour for accurate springback predictions. Int J Mech Sci 51:547–563
8. Kim H, Kimchi M (2011) Numerical modeling for springback prediction by considering the variation of elastic modulus in stamping advance high-strength steel. In: The 8th international conference and workshop on numerical simulation of 3D sheet metal forming process. (1383) 1159-1166
9. Verma RK, Chung K, Kuwabara T (2011) Effect of pre-strain on anisotropic hardening and springback behaviour of an ultra-low carbon automotive steel. ISIJ Int 51:482–490
10. Fleischer M, Borrvall T, Bletzinger, KU (2007) In: Proceeding of the 6th European LS-DYNA Users Conference, 141–152
11. Yu HY (2009) Variation of elastic modulus during plastic deformation and its influence on springback. Mater Des 30:846–850
12. Chongthairungruang B, Uthaisangsuk V, Suranuntchai S, Jirathearanat S (2012) Experimental and numerical investigation of springback effect for advanced high strength dual phase steel. Mater Des 39:318–328
13. Zhu H, Huang L, Wong C (2004) Unloading modulus on springback in steels, Society of Automotive Engineering
14. Yoshida F, Uemori T (2002) A model of large-strain cyclic plasticity describing the Bauschinger effect and work hardening stagnation. Int J Plast 18:661–686
15. Zang S, Lee M, Kim J (2013) Evaluating the significance of hardening behavior and unloading modulus under strain reversal in sheet springback prediction. Int J Mech Sci 77:194–204
16. Eggertsen PA, Mattiasson K (2010) On constitutive modeling of springback analysis. Int J Mech Sci 52:804–818

17. Xu WL, Ma CH, Li CH, Feng WJ (2004) Sensitive factors in springback simulation for sheet metal forming. J Mater Process Tech 151:217–222

18. Lee S W, Yang D Y (1998) An assessment of numerical parameters influencing springback in explicit finite element analysis of sheet metal forming process. J Mater Process Tech. (80-81):60-67

19. Samuel M (2000) Experimental and numerical prediction of springback and side wall curl in U-bendings of anisotropic sheet metals. J Mater Process Technol 105(3):382–393

20. L Papeleux, J P Ponthot (2002) Finite element simulation of springback in sheet metal forming. J. Mater. Process. Technol. (125-126): 785–791.

21. Y Ledoux, E Pairel, R Arrieux, P Teixeira, A D Santos, J Duarte (2005) A method of springback and tool compensation based on finite element method and design of experiment. Proceedings of the IDDRG conference, 390–399

22. Alves de Sousa et al (2008) Unconstrained springback behavior of Al–Mg–Si sheets for different sitting times. Int J Mech Sci 50: 1381–1389

23. D'Acquisto L, Fratini L (2006) Springback effect evaluation in three-dimensional stamping processes at the varying of blankholder force. Proc Inst Mech Eng Part B J Eng Manuf 220:1827–1837

24. Hirose Y, Kojima M, Ujihara S, Hishida U (1992) Development of forming technique with real-time control of blank holding force. Proceedings of the IDDRG conference, 300– 307

25. Cao J, Kinsey B, Solla SA (1999) Consistent and Minimal Springback Using a Stepped Binder Force Trajectory and Neural Network Control. J Eng Mater Technol 122:113–118

26. Schmoeckel D, Beth M (1993) Springback Reduction in Draw-Bending Process of Sheet Metals. CIRP Ann - Manuf Technol 42: 339–342

27. Liu G, Lin Z, Bao Y (2002) Improving dimensional accuracy of a u-shaped part through an orthogonal design experiment. Finite Elem Anal Des 39:107–118

28. Liu G, Lin Z, Xu W, Bao Y (2002) Variable blankholder force in U-shaped part forming for eliminating springback error. J Mater Process Technol 120:259–264

29. ul Hassan H, Fruth J, Güner A, Tekkaya A E (2013) Finite element simulations for sheet metal forming process with functional input for the minimization of springback. Proceedings of the IDDRG conference, 393-398

30. Kitayama S, Yoshioka H (2014) Springback reduction with control of punch speed and blankholder force via sequential approximate optimization with radial basis function network. Int J Mech Mater Design 10:109–119